

*The Astrophysical Journal; resubmitted January 17, 2001*

## The kinematics of 3:1-merger remnants and the formation of low-luminosity elliptical galaxies

N. Cretton, T. Naab, Hans-Walter Rix, A. Burkert

*Max-Planck-Institut für Astronomie, Königstuhl 17, Heidelberg, Germany*

### ABSTRACT

We test the formation of low-luminosity elliptical galaxies through collisionless mergers of unequal-mass disk galaxies. The kinematic properties of a small survey of simulated merger end-products with initial disk mass ratios of 3:1 is compared to a sample of seven low-luminosity galaxies observed by Rix et al. that were chosen photometrically to be "ellipticals". In this paper, we go beyond a comparison in terms of global properties (using one number to characterize a model or a galaxy e.g.,  $\langle a_4 \rangle$ , ellipticity at some fixed radius or central velocity dispersion) and examine the detailed kinematics as function of galactocentric distance. The merger remnants are "observed" through a slit along the major and minor axis, using a pixel binning and slit width similar to the one used during the spectroscopic observations. Inside each bin, we determine the line-of-sight velocity distributions and parametrize them with Gauss-Hermite functions. We compare the rotational support of the merger remnants, i.e., the ratio of the mean line-of-sight velocity  $v$  to the velocity dispersion  $\sigma$  along the major axis, the normalized rotation on the minor axis and the major axis Gauss-Hermite moments  $h_3$ , to that of the observed galaxies.

The N-body remnants are very flattened when viewed edge-on ( $\langle \epsilon \rangle \sim 0.6$ ) and should be inclined before making a fair comparison with the Rix et al. data set (which has  $\langle \epsilon \rangle \sim 0.3$ ). When the merger remnants are appropriately inclined, their  $v/\sigma$  profiles rise slower than the observed ones:  $v/\sigma_{\text{merger}}$  is in the range [0.1, 0.8] at  $1 R_{\text{eff}}$  and [0.2, 1.6] at  $2 R_{\text{eff}}$ , whereas the  $v/\sigma_{\text{observed}}$  span the intervals [0.8, 2.0] at  $1 R_{\text{eff}}$  and [1.4, 3.5] at  $2 R_{\text{eff}}$ . Note that even when the remnants are viewed edge-on, the  $v/\sigma$  profiles do not match the observations.

The detailed comparison of the observations with our set of purely collisionless 3:1-merger remnants shows that these objects and low-luminosity ellipticals do not have similar kinematic profiles. This suggests that this kind of dissipationless merger (or mergers with more even masses, e.g., mass ratios of 2:1 or 1:1) is not likely to be the dominant formation channel for low-luminosity elliptical galaxies.

*Subject headings:* galaxies: elliptical and lenticular, cD — galaxies: kinematics and dynamics — galaxies: structure.

## 1. Introduction

Elliptical galaxies can be divided into two classes according to their morphology and kinematic properties. The giant ellipticals are generally boxy (probably triaxial) with shapes supported by anisotropy. They have slow rotation on the major axis with often comparable minor axis rotation, and occasionally kinematically decoupled cores. The intermediate and low-luminosity ellipticals are usually disky, isotropic rotators. They are mostly supported by rotation and have little minor axis velocities (Bender 1988; Bender, Döbereiner & Möllenhoff 1988; Kormendy & Bender 1996; Rix et al. 1999). These two families also show correlations with the inner slope of the surface brightness profile: galaxies with steep inner cusps are on average small disky objects and galaxies with shallow or constant cores are the giant boxy ellipticals (Jaffe et al. 1994, Faber et al. 1997, Carollo et al. 1997).

Barnes (1998) proposed that fast rotating elliptical galaxies could originate from collisionless merger of unequal-mass disks. On the other hand, equal-mass mergers lead to slowly rotating, pressure supported objects resembling giant elliptical galaxies (Barnes 1992). Recently Naab, Burkert & Hernquist (1999, hereafter NBH) took Barnes' idea one step further and showed that equal and unequal-mass mergers could reproduce most of the observed correlations mentioned above if one would analyse projections of the merger remnants using many random viewing angles (see their figure 3). They showed that the boxy family of galaxies could be explained by equal-mass mergers of disk galaxies (with bulges and dark halos), whereas the disky family was originating from 3:1 mergers, i.e., in which the big disk galaxy is 3 times more massive than the small one.

However, NBH's conclusion is based only on global properties (average  $a_4$ , ellipticity measured at one radius, or central velocity dispersion) and does not compare kinematic quantities *as function of radius*. In this paper, we perform such a comparison, using a setup similar to the one used during the observations of Rix et al. 1999 (hereafter R99), where kinematics along the principal axes were obtained, extending well beyond  $R_{\text{eff}}$ . R99 selected these elliptical galaxies only on the basis of their low-luminosities ( $M_B \geq -19.5$ ), i.e., no prior kinematic information or degree of diskiness was used.

In section 2, we summarize our merger models and their initial conditions. In section 3, we describe how we extract the kinematic quantities of the merger remnants. We discuss the results of a small survey of 16 different merger remnants in section 4. We perform a comparison between models and observations using the rotational support (i.e.,  $v/\sigma$  along the major axis, the amount of minor to major axis rotation and the Gauss-Hermite moment  $h_3$  along the major axis. All these quantities are compared as function of distance from the center. The edge-on and inclined merger models fail to match the observed quantities of the R99 sample.

In a similar study, Bendo & Barnes (2000, hereafter BB) examined 8 equal-mass merger remnants and 8 unequal-mass (3:1) merger remnants. Their unequal-mass merger models display similar major axis kinematic profiles than ours. However, the authors reach different conclusions from the comparison with the R99 data set, namely that "unequal-mass merger mergers can produce the same relations between  $v/\sigma$  and radius". In this paper, we do a more direct comparison of N-body merger remnants with this data set. We compare not only edge-on but also inclined remnants that

match the apparent ellipticities of the observed galaxies. We conclude that, on average, the kinematics of the simulated 3:1 mergers do not reproduce those of low-luminosity galaxies. Therefore we suggest that the 3:1 collisionless mergers are probably not a major mechanism responsible for the bulk formation of these objects.

## 2. The merger models

We briefly summarize some properties of the initial disk model (see Hernquist 1993 and NBH for more details). Each disk galaxy consists of an exponential disk, a Hernquist (1990) spherical bulge and a pseudo-isothermal spherical dark halo with 5.8 times the mass of the disk. In our "low-resolution" simulations, the more massive galaxy has 6666 bulge particles, 20000 disk particles and 40000 dark halo particles, while the less massive galaxy has a third of the number of particles in each component. In two "high-resolution" cases, we rerun models with three times as many particles. The N-body computations were performed using a direct summation code on the special purpose hardware GRAPE-3 AF (GRavity PipE, Sugimoto et al. 1990).

Before the encounter, the two disk galaxies follow a quasi-parabolic orbit with an initial separation of 30 scale-lengths of the massive exponential disk. The pericentric approach is taken as 2 disk scale-lengths. Once the orbits and the masses of the two initial spiral galaxies are fixed, we still have 2 free parameters for each galaxy: the inclination between the galaxy orbital plane and its spin plane (angle  $i$ ) and the argument of pericenter (angle  $\omega$ ), i.e., the angle between the line of nodes and the pericentric distance (see Figure 6a of Toomre & Toomre, 1972). Table 1 summarizes our choice for these angles:  $i_1, \omega_1$  for the more massive spiral galaxy and  $i_2, \omega_2$  for the less massive one.

## 3. Observing the merger remnant

We analyse the kinematic structure of the merger remnants 10 dynamical times after the merger has been completed, so that they had enough time to settle into an equilibrium state. We plot the kinematic quantities of the remnant in units of the half-light radius  $R_{\text{eff}}$ , i.e., the projected radius on the plane of the sky of the circle containing half of the luminous particles. The average  $R_{\text{eff}}$  of the R99 data set is  $\sim 13''$ , corresponding to 3.34 kpc. In the merger remnants, 1  $R_{\text{eff}}$  is 3.5 kpc: this distance is chosen to be  $10''$  for the comparison with observations. We use a slit width of  $2.5''$ , i.e., 0.875 kpc. After binning, we have 21 pixels on the major axis and 16 on the minor axis. The bin size increases with distance from the center, according to the observations of R99.

In each binned pixel, we construct the histograms of the line-of-sight velocities ( $v_{\text{los}}$ ) of all the luminous particles whose projected coordinates on the sky ( $x'$  and  $y'$ ) fall within the pixel boundaries. This quantity is called the velocity profile (VP). Subsequently, we parametrize the VPs using Gauss-Hermite series (van der Marel & Franx 1993, Gerhard 1993). We checked that the kinematic parameters of each VP ( $v, \sigma, h_3$  and  $h_4$ ) do not depend on the choice of the velocity bin size. Furthermore, to increase the signal to noise and since most remnants are close to an

axisymmetric shape (in the equatorial plane, the average axis ratio at  $1R_{\text{eff}}$  is roughly 0.8–0.9), we average the results over 10 different position angles of the slit between  $0^\circ$  and  $90^\circ$  in the equatorial plane. Figure 4 and 5 demonstrate that the results of this paper still hold if we considered individual projected profiles, rather than averaging 10 position angles together.

We estimate the errors on each kinematical quantities by bootstrapping. For each spatial bin, we generate 100 bootstrapped VPs and recompute the GH-decomposition. The error bar is then estimated as the variance amongst the 100 bootstrapped results.

In Figure 1, we show the basic kinematic output of our simulations, the first four moments of the VPs, i.e.,  $v, \sigma, h_3, h_4$  and the degree of ordered motion  $v/\sigma$  on the major axis for the high resolution simulation (266666 luminous and dark particles) of case 1 (see table 1). The initial inclination angles of the two disk galaxies are  $[i_1, \omega_1, i_2, \omega_2] = [-30, -30, 30, 30]$ . The curves have been folded onto the positive side of the major axis (with a sign change for the odd moments  $v$  and  $h_3$ ). In this way, we can estimate the left/right asymmetries. In most geometries analysed in this paper, the left and right side of the major axis are similar within the errors. For this model, the mean velocity increases linearly until  $1 R_{\text{eff}}$  and then rises more slowly to reach  $150 \text{ km s}^{-1}$  at  $3 R_{\text{eff}}$ . In other geometries, the rise is more monotonic but reaches the same value at  $3 R_{\text{eff}}$ . The velocity dispersion decreases from central values of  $140\text{--}160 \text{ km s}^{-1}$  to  $80\text{--}100 \text{ km s}^{-1}$  at  $3 R_{\text{eff}}$ . The innermost point shows a lower value (by  $\sim 20 \text{ km s}^{-1}$ ) compared to its immediate neighbors. BB observed the same behavior in their simulations and interpreted it as follows: all the merger remnants have a large fractions of particles from the Hernquist bulges of their progenitors in their inner regions. These particles still follow a  $r^{-1}$  density profile at small radii and therefore have velocity dispersion that scale as  $r^{-1/2}$ , producing the central dip.

In Figure 2 and 3, we show the  $v/\sigma$  and  $h_3$  profiles of two cases, where each simulation was rerun with three times more particles. The low resolution simulations (with 88887 particles) do not show significantly different results compared to the high resolution cases. In case 1, the low resolution models have more left/right asymmetry, but if one takes the average between the two sides, then the  $v/\sigma$  and  $h_3$  profiles are very similar. Therefore in the remainder of this paper, we will explore various initial conditions using only low resolution simulations. Similarly, Figure 3 displays the  $h_3$ -profiles for the high/low resolution simulations:  $h_3$  is typically zero or positive inside  $1 R_{\text{eff}}$  (see also BB).

## 4. Discussion

### 4.1. Edge-on remnants

Figure 6 overplots the observed  $v/\sigma$  profiles of the R99 sample and the  $v/\sigma$  profiles of all our merger models (see table 1) when viewed edge-on. In the models, the left and the right sides have been averaged. The  $v/\sigma$  profiles of the remnants can reach values between 1 and 2.2 in the very outer parts i.e., at  $3 R_{\text{eff}}$ . At smaller radii, e.g., at  $1 R_{\text{eff}}$ , they attain only  $[0.1, 1.0]$ , depending on the geometry. BB find similar results for their 3:1 merger remnants, as indicated by the shaded region in Figure 6. The R99 data set shows higher values of  $v/\sigma$  at all radii: at  $1 R_{\text{eff}}$   $v/\sigma_{\text{observed}}$

covers the range [0.8, 2.0] and [1.4, 3.5] at  $2 R_{\text{eff}}$ . Note also the sharp increase in  $v/\sigma_{\text{observed}}$  at small radii ( $R \leq 0.5 R_{\text{eff}}$ ). Furthermore the merger simulations do not reproduce the central peak in  $\sigma$  observed by R99 (see their Figure 1). From this comparison alone we could conclude that dissipationless simulations can not reproduce the observed kinematics of the R99 sample. In the next section, we will also use the GH-moment  $h_3$  and the minor axis rotation to compare with the observations.

#### 4.2. Inclined remnants

When viewed edge-on, our merger remnants have an apparent ellipticity  $\epsilon_{\text{remnant}} \simeq 0.5 - 0.6$  at  $1 R_{\text{eff}}$ , much more flattened than the objects of R99 with  $\langle \epsilon_{\text{observed}} \rangle = 0.3$  (see their Figure 3). In order to make a fair comparison to this dataset, we need to incline our merger remnants such that they have the same ellipticity  $\epsilon_{\text{remnant}} \simeq 0.3$  at  $1 R_{\text{eff}}$ . As can be expected, the mean line-of-sight velocity is lowered (compared to the edge-on case). The velocity dispersion is also diminished, but not as much as the velocity. Therefore the  $v/\sigma$  profiles of the inclined cases do not rise as fast as the edge-on cases (Figure 7).

The  $h_3$ -profiles are less sensitive to inclination, i.e., they are similar to those of the edge-on case. In Figure 8, we only show the  $h_3$  values of the merger remnants in the inclined case. These profiles are essentially zero (or slightly positive) inside  $1 R_{\text{eff}}$ , whereas the observed  $h_3$  values show an outward decline towards  $\langle h_3 \rangle = -0.06$  within the same radial interval. The model values reach  $-0.1$  only at very large radii ( $3 R_{\text{eff}}$ ). Bender, Saglia & Gerhard (1994) observed a sample of 44 elliptical galaxies and found  $\langle h_3 \rangle = -0.1$  for the disk-like ( $a_4/a = 0.02$ ) objects (see their Figure 14a). We choose the disk-like subsample, since they correlate with the low-luminosity ellipticals. Their low values of  $h_3$  is roughly consistent with the R99 profiles, since Bender, Saglia & Gerhard obtained spectra only inside  $1/2 R_{\text{eff}}$ .

#### 4.3. Minor axis rotation

We have computed the normalized minor axis rotation, defined as  $v_{\text{min.norm.}} = v_{\text{minor}} / \sqrt{v_{\text{major}}^2 + \sigma_{\text{major}}^2}$  for all merger models and observations. Note that the normalization by the total kinetic energy avoids a division by zero in the center. We find that both the merger remnants and the galaxy sample observed by R99 have only a small amount of minor axis rotation:  $\langle v_{\text{min.norm.}} \rangle_{\text{merger}} = 0.04$  and  $\langle v_{\text{min.norm.}} \rangle_{\text{R99}} = 0.08$ . The spatial average has been done inside  $2 R_{\text{eff}}$ .

#### 4.4. Comparison with S0 galaxies

Fisher (1997) observed a sample of 18 S0 galaxies and derived GH-moments along their major and minor axis. In most cases, these major axis  $h_3$  profiles show a similar behavior than observed in

our merger remnants: going from the center to the outer parts,  $h_3$  values increase from zero to some positive values, then decrease and change sign to finally remain negative. The maximum value of  $h_3$  reached by the data is in the range 0.05–0.1. However, the change of sign occurs at (or within)  $1 R_{\text{eff}}$  for these S0s, whereas it is between 1 and  $2 R_{\text{eff}}$  for the merger remnants. Furthermore, the shape of the S0s velocity curves is very different compared to the one of the merger remnants (see Figure 10 of Fisher) and their  $v/\sigma$  values are even higher than the low-luminosity ellipticals.

#### 4.5. Kinematic temperature of the initial galaxy disk

The merging process heats up the disks (i.e., increases  $\sigma$ ), decreases  $v$  and therefore lowers the  $v/\sigma$  profile. Among other comparisons in this paper, we reject the merging scenario because we were unable to reproduce the observed  $v/\sigma$  values, but this scenario might be viable if the initial disks were colder. Therefore it is interesting to know the *initial* temperature of the disk before the merger. In Figure 9 (bottom panel), we show this initial  $v/\sigma$  profile of the largest disk galaxy. It rises linearly with radius and reaches  $v/\sigma = 7.5$  at 3 disk scale length along the major axis (edge-on view). The initial disk galaxy has a bulge to disk mass ratio of 1/3, so it compares to a Sb galaxy (see e.g., Figure 4.51 of Binney & Merrifield 1998). For comparison, the old stellar population of Milky Way galaxy (SBb) reaches  $v/\sigma \simeq 4$  at the Sun position (2.5 disk scale length). We computed the  $v/\sigma$  profile for six Sa galaxies from Corsini et al. (1999); they reach  $v/\sigma = 2$  at one disk scale length  $R_{\text{exp}}$  and  $v/\sigma = 4$  at two  $R_{\text{exp}}$  with large error bars in the outer parts. The inclination  $i$  does not play a role here since  $v/\sigma$  is almost independent of  $i$ , when  $i \leq 50$  away from edge-on. Bottema (1999) has measured velocity and velocity dispersion for the Sb galaxy NGC 7331 up to  $3 R_{\text{eff}}$ . The  $v/\sigma$  profile of that galaxy reaches values around 8 at  $3 R_{\text{eff}}$ , but has a steeper inner slope: at  $1 R_{\text{eff}}$ , NGC 7331 has  $v/\sigma = 4$  already. We have started a merger simulation with a colder initial disk using the geometry of case 1 (see table 1). We find virtually the same  $v/\sigma$  profile in the remnant of the merger simulation (see Figure 9, top panel). We conclude that our choice of initial galaxy disk is not an artificial cause for the low  $v/\sigma$  profile found in our merger remnants.

### 5. Could small ellipticals still be merger products?

In this section, we speculate on some possible scenarii that could still save the 3:1 merger of disks as a viable route for the formation of fast rotating ellipticals. In addition, one (non-merger) mechanism is mentioned that could also lead to the formation of similar objects.

If we start with a sub-maximal initial disks, a weaker bar instability occurs since massive dark halos tend to stabilize disks against bars. Therefore the disks are less heated during the merger and could produce a remnant with a higher  $v/\sigma$  profile, in agreement with the R99 sample. Using a fast-rotating bulge in the initial spiral galaxy could increase the  $v/\sigma$  profile of the remnant in the inner parts. Finally, the inclusion of a dissipative component in the merger is also likely to increase the amount of ordered motion: in gas-rich 3:1 merger simulations, large ( $\sim 1 R_{\text{eff}}$ ) gaseous disks form in the remnant (Naab 2000). If new stars are subsequently formed in such disks, the final

rotational support is increased. It is however not clear what fraction of the gas is turned into stars (and under what conditions and timescale).

In a cluster environment, mergers occur rarely since the velocity dispersion is too high. However, galaxy harassment is likely to play a significant role. According to Moore, Lake & Katz (1998) disks galaxies in rich clusters undergo a complete morphological transformation from "disks" to "spheroidals". These objects probably retain a large amount of rotation and may therefore have a high  $v/\sigma$ .

Finally, we have compared our merger remnants with the low-mass end of the elliptical sequence. Intermediate ellipticals ( $-19 < M_B < -20$ ) show more modest  $v/\sigma$  profiles. The kinematics of these objects may still be explained by 3:1 collisionless mergers.

## 6. Conclusions

We have compared various kinematic characteristics of a limited sample of 3:1 N-body merger remnants with observations of low-luminosity elliptical galaxies in order to test if the collisionless merger of disk galaxies (with mass ratio of 3:1) are a likely formation mechanism for such objects. The simulated merger remnants and the observed galaxies both show rapid rotation along the major axis and little rotation along the minor axis. A detailed comparison between simulations and data shows, however, that on average, the rotational support  $v/\sigma$  of the simulated remnants is too small compared to the observed galaxies. A comparison of the line-of-sight VP, quantified by  $h_3$ , reveals that the merger remnants have VPs with zero or positive  $h_3$  inside  $1 R_{\text{eff}}$ , whereas the observed VPs have  $\langle h_3 \rangle \simeq -0.06$  in the same interval. These more direct comparisons with the data support the conclusion of R99 based on simpler models, i.e., the low-luminosity galaxies have a different dynamics than the 3:1 merger remnants. In particular they have, on average, more ordered motion. These conclusions differ from the ones reached by BB, even though the results of our simulations agree with theirs. The difference can be traced to the more detailed and rigorous data model comparison performed here.

At face value this suggests that either the last merger that this class of small "ellipticals" experienced had a mass ratio  $> 3:1$ , or that a substantial stellar disk formed by gas dissipation after the last major merger. Note that we have been conservative by looking at 3:1 mergers in the sense that the 3:1 remnants are the most likely objects to look like an elliptical and have a high rotation support: 1:1 mergers lead to boxy objects with far less rotation support and 5:1 mergers (or higher) do not form an elliptical because the large disk mostly survive the interaction. It is not clear quantitatively what is the effect of the inclusion of gas and star formation in the kinematics of the remnant. Furthermore, adding gas might not be the only way to save the merging scenario. For example, starting the merger with a sub-maximal disk could produce a remnant with a higher  $v/\sigma$  profile. On the other hand, galaxy harassment is a plausible mechanism to heat the disk of spirals, while keeping some degree of ordered motion. However harassment is mainly operating in rich clusters, whereas mergers are ubiquitous in a hierarchical formation scenario.

We thank Josh Barnes for his constructive comments on the manuscript.

## REFERENCES

Barnes, J. E. 1992, *ApJ*, 393, 484

Barnes, J. E., in *Galaxies: Interactions and Induced Star Formation*, ed. D. Friedli, L. Martinet & D. Pfenniger (Saas-Fee Advanced Course Lecture Notes, No. 26; Berlin: Springer), 275

Bender, R. 1988, *A&A*, 193, L7

Bender, R., Döbereiner, S., & Möllenhoff, C. 1988, *A&AS*, 74, 385

Bender, R., Saglia, R. P., Gerhard, O. E. 1994, *MNRAS*, 269, 785

Bendo, G., Barnes, J. 2000, *MNRAS*, in press, (astro-ph/0003248)

Bottema, R. 1999, *A&A*, 348, 77

Carollo, C. M., Franx, M., Illingworth G. D., Forbes D. 1997, *ApJ*, 481, 710

Corsini, E. M., Pizzella, A., Sarzi, M., Cinzano, P., Vega Beltran, J. C., Funes, J. G., Bertola, F., Persic, M., & Salucci, P. 1999, *A&A*, 342, 671

Faber, S. M., et al. 1997, *AJ*, 114, 1771

Gerhard, O. E. 1993, *MNRAS*, 265, 213

Hernquist, L. 1993, *ApJS*, 86, 389

Jaffe, W., Ford, H. C., O'Connell, R. W., van den Bosch, F. C., Ferrarese, L. 1994, *AJ*, 108, 1567

Kormendy, J., & Bender, R. 1996, *ApJ*, 464, L119

Moore, B., Lake, G., & Katz, N. 1998, *ApJ*, 495, 139

Naab, T., Burkert, A., & Hernquist, L. 1999, *ApJ*, 523, L133

Naab, T. 2000, *Galaxy Disks and Disk Galaxies*, ASP Conference Series, Vol.  $3 \times 10^8$ , J. G. Funes S. J., and E. M. Corsini, eds.

Rix, H.-W., Carollo, C. M., Freeman, K. C. 1999, *ApJ*, 513, L25

Sugimoto, D., Chikada, Y., Makino, J., Ito, T., Ebisuzaki, T., & Umemura, M. 1990, *Nature*, 345, 33

Toomre, A., & Toomre, J. 1972, *ApJ*, 178, 623

van der Marel, R. P., & Franx, M. 1993, *ApJ*, 407, 525

Table 1. Angles specifying the initial conditions for the two disk galaxies

$i$ (1)	$i_1$ (2)	$\omega_1$ (3)	$i_2$ (4)	$\omega_2$ (5)
1	-30	-30	30	30
2	90	0	0	0
3	0	0	0	0
4	180	0	0	0
5	-71	90	109	90
6	30	0	0	0
7	60	0	0	0
8	-90	90	90	90
9	-30	0	0	0
10	-60	0	0	0
11	60	60	-60	-60
12	120	0	0	0
13	150	0	0	0
14	-120	-30	60	-30
15	60	-30	-120	-30
16	60	30	-60	-30

Note. — Column (1) gives the number of the simulation, column (2) the angle between the spin plane and the orbital plane for the massive disk galaxy and column (3) the angle between the line of nodes and the pericenter. Column (4) and (5) are the same than (2) and (3), but for the small spiral galaxy.

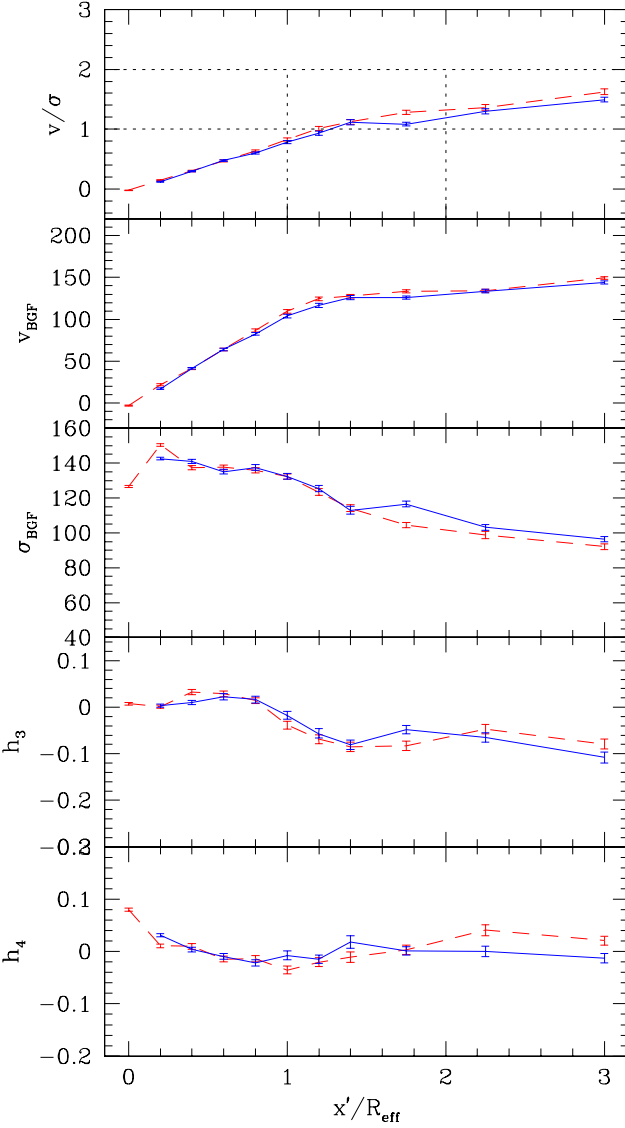


Fig. 1.— First four moments of the GH decomposition along the major axis of one merger remnant (case 1, see table 1): mean line-of-sight velocity  $v$  (in km/s), line-of-sight velocity dispersion  $\sigma$  (in km/s) and GH-moments  $h_3$  and  $h_4$ . The top panel shows the rotational support, i.e., the ratio  $v/\sigma$ . The remnant is viewed edge-on here. The left side of the remnant (dashed line) has been folded onto the right side to estimate the asymmetry.

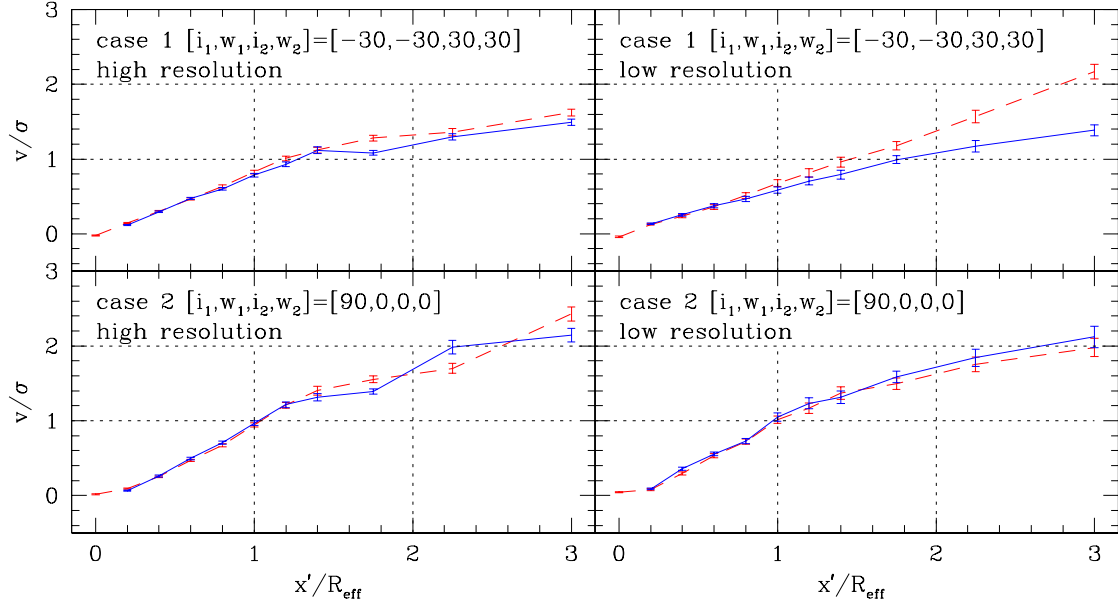


Fig. 2.—  $v/\sigma$  profiles for the first two geometries. The left panels show simulations with three times more particles than those in the right panels. All profiles are viewed edge-on.

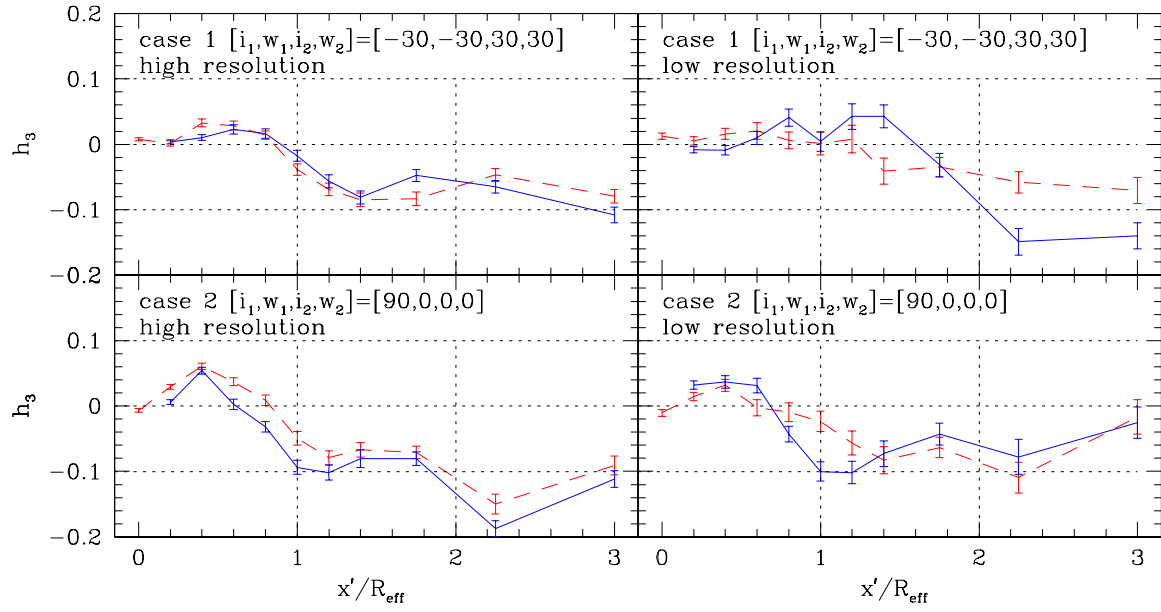


Fig. 3.— Same as Figure 2, but for  $h_3$ .

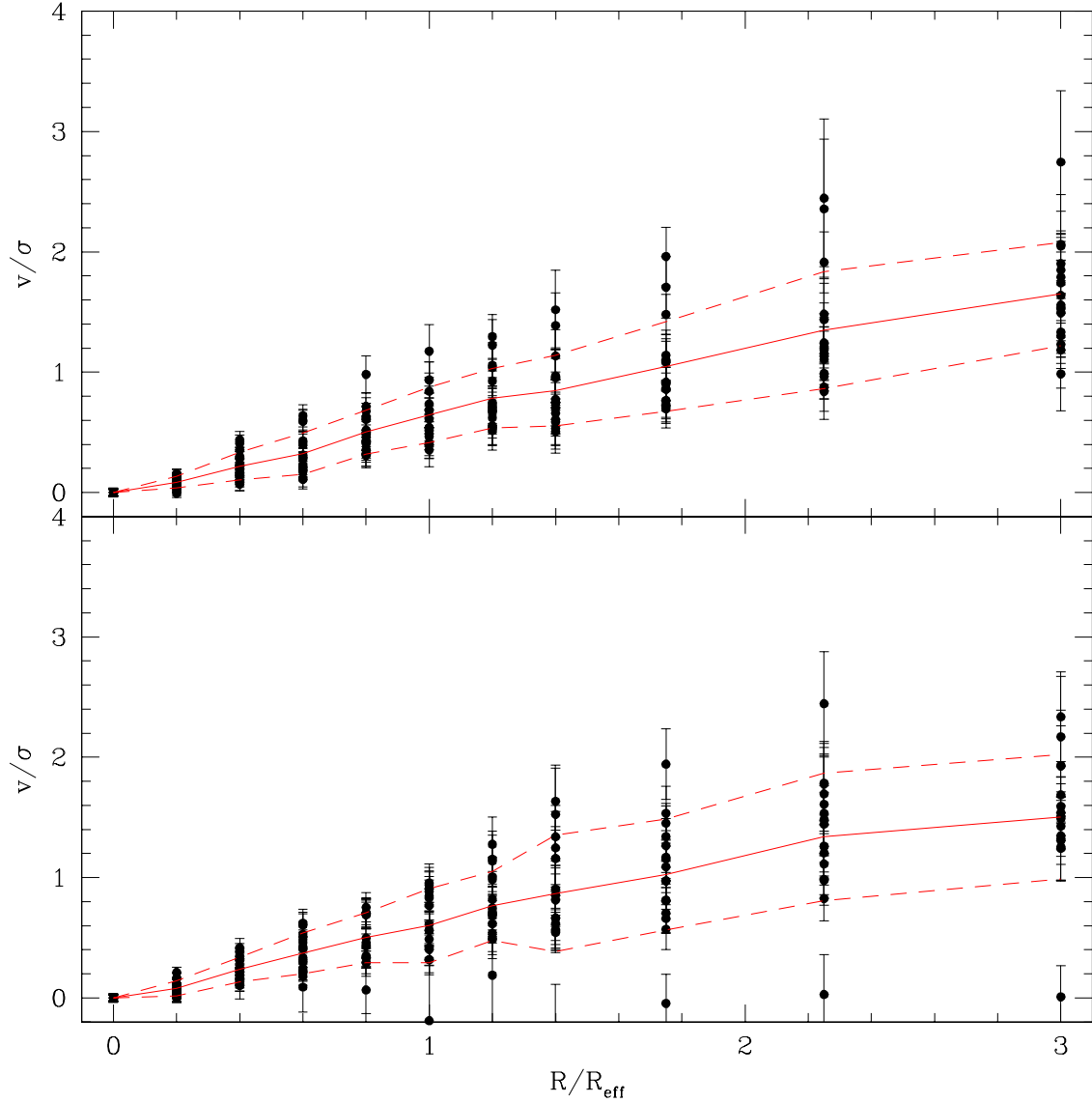


Fig. 4.—  $v/\sigma$  profiles viewed edge-on for all the merger simulations. Here no azimuthal average is performed: the bottom panel shows the results measured along the  $x$ -axis and the top panel along the  $y$ -axis in the equatorial plane. The full line is the average profile, while the two dashed lines show the  $1\sigma$  band. On average both distributions are identical, so we conclude that the results are independent of the viewing angle.

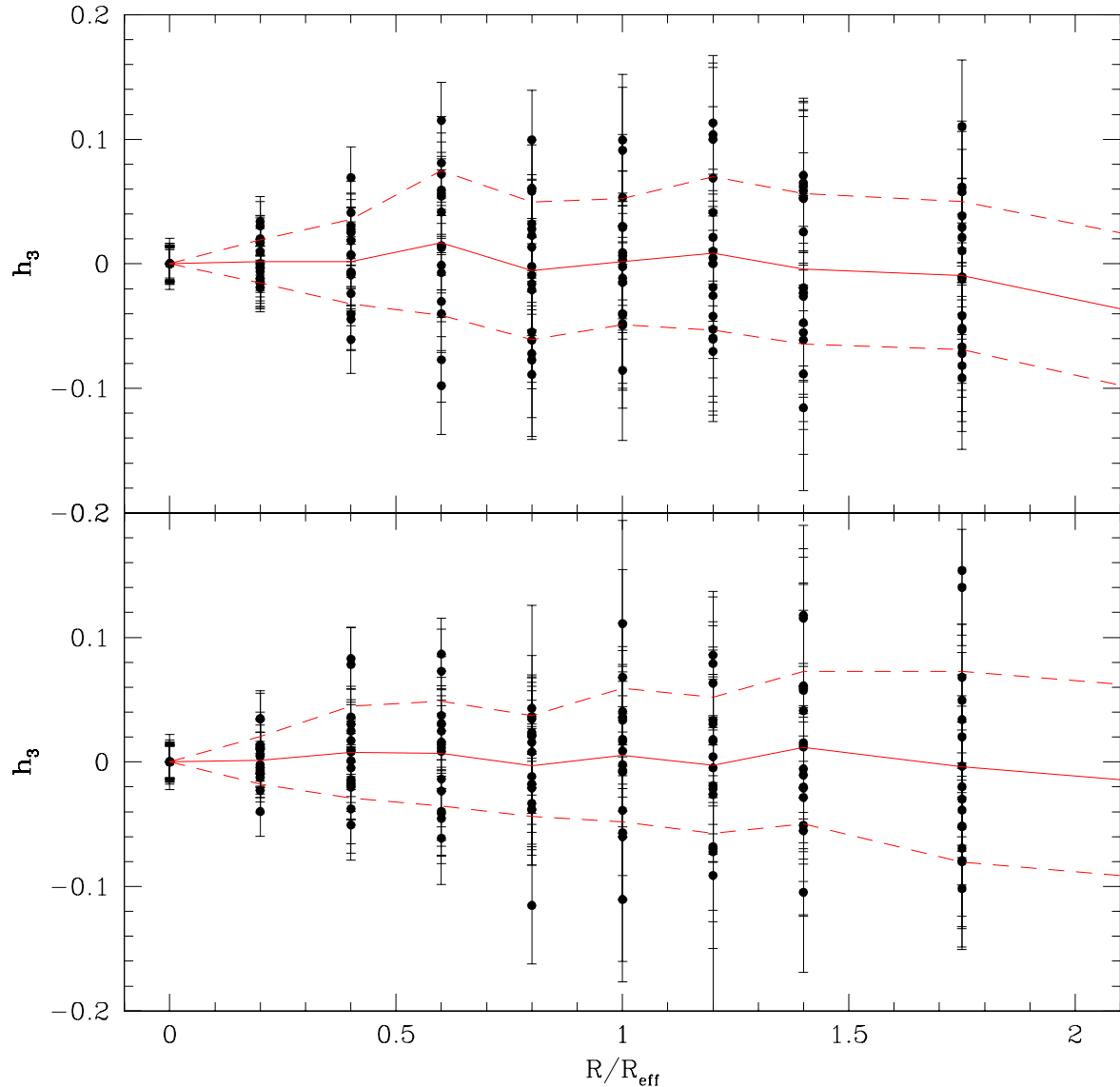


Fig. 5.— Same as Figure 4, but for  $h_3$ .

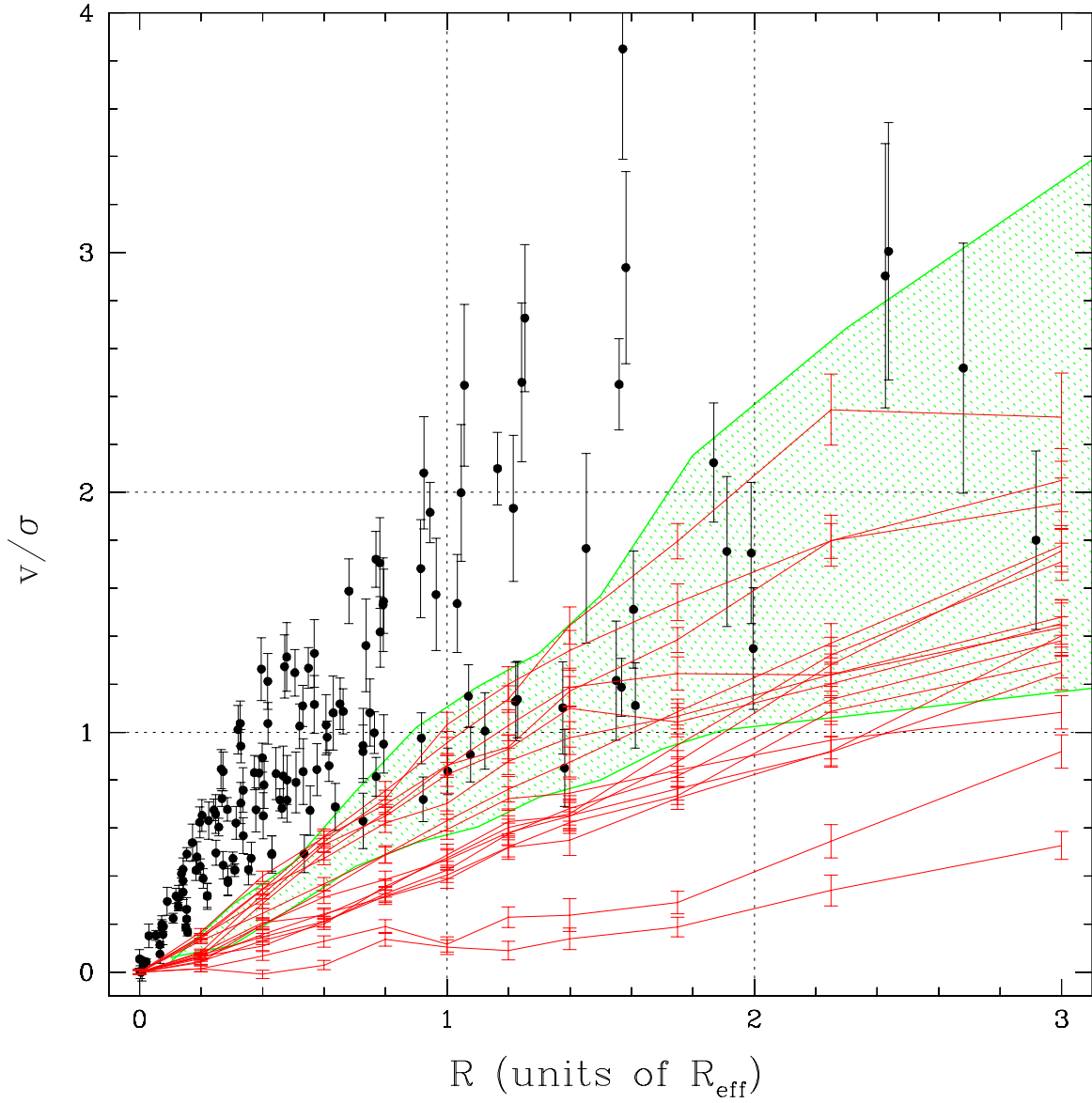


Fig. 6.— Comparison of observed  $v/\sigma$  (filled dots with error bars) and  $v/\sigma$  for the edge-on merger remnants (lines with error bars). The shaded area corresponds to the range occupied by the edge-on models of BB. Both distributions are not compatible with the observed one, even in this edge-on case.

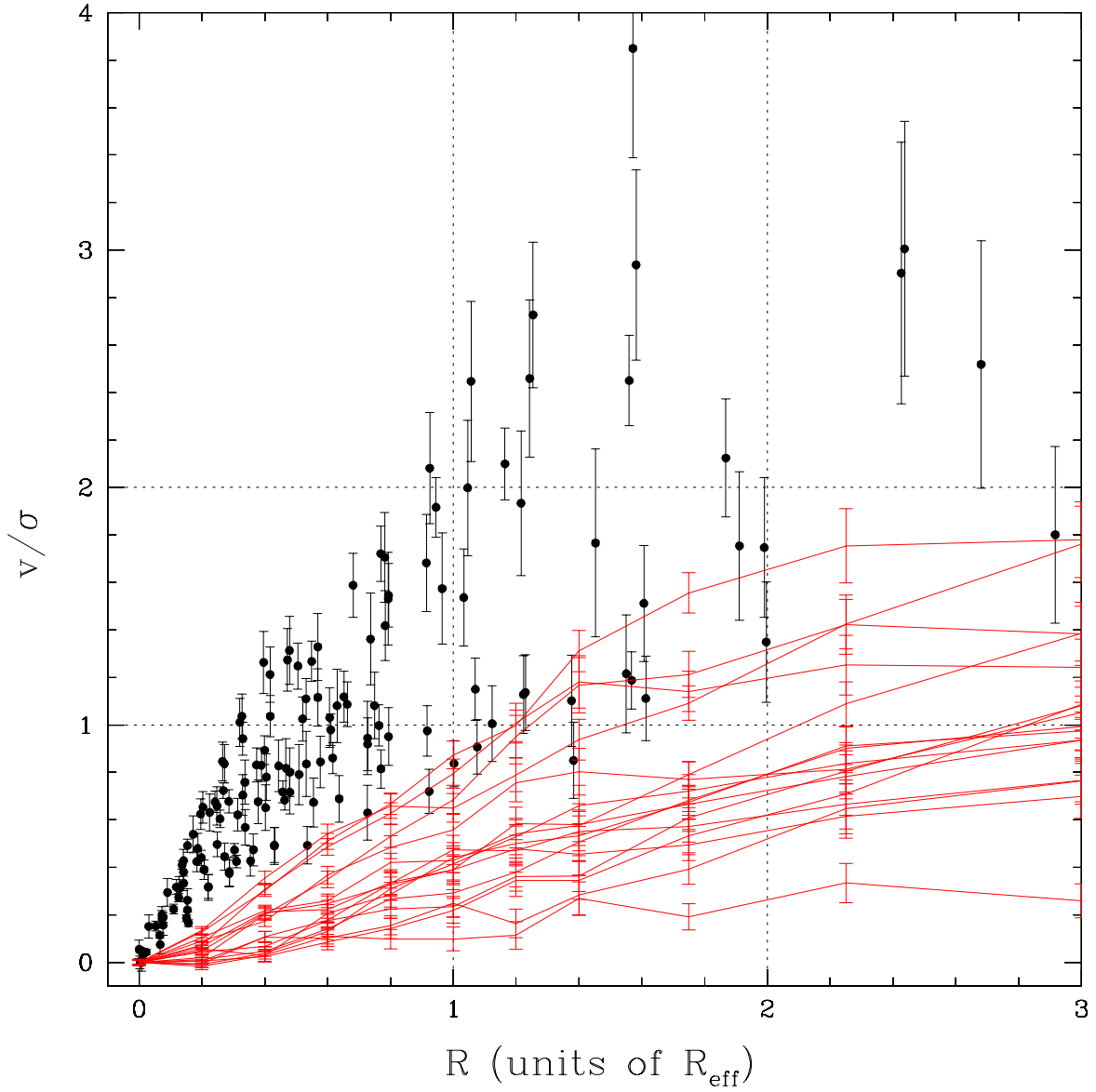


Fig. 7.— Same as Figure 6, but with inclined merger remnants. The inclinations are chosen such that each merger remnant has an apparent  $\epsilon = 0.3$ , which is the average value of the R99 sample.

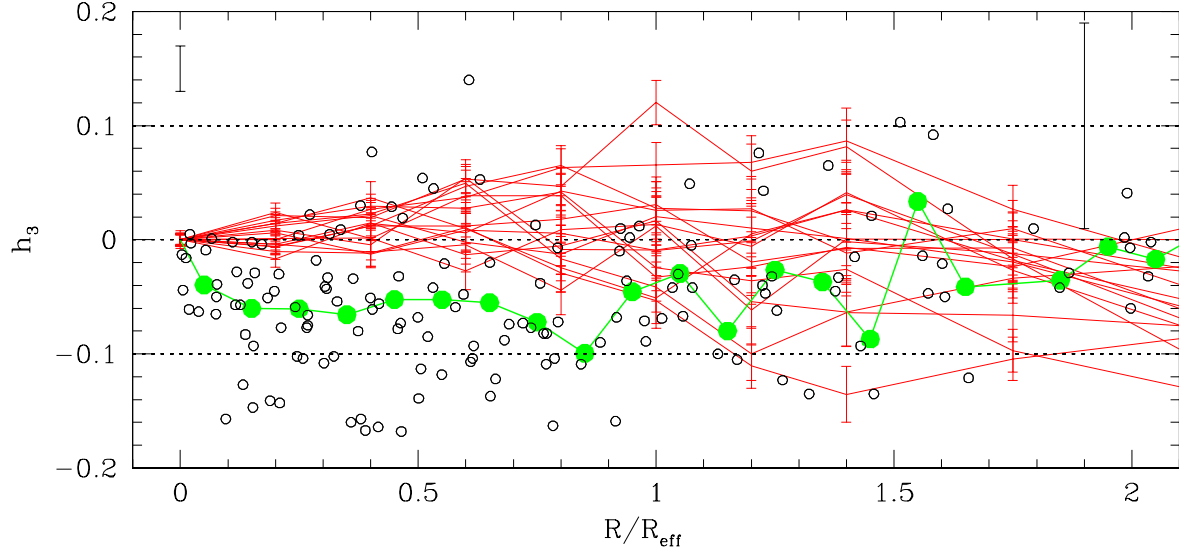


Fig. 8.— Same as Figure 7, but for  $h_3$ . The big filled dots are the average profile of the observations and the small open dots are the observed  $h_3$  data points. Outside  $1 R_{\text{eff}}$ , the error bars become too large to make a meaningful comparison. A typical error bar is reproduced in the upper left (for the center) and right (for the outer parts) corners.

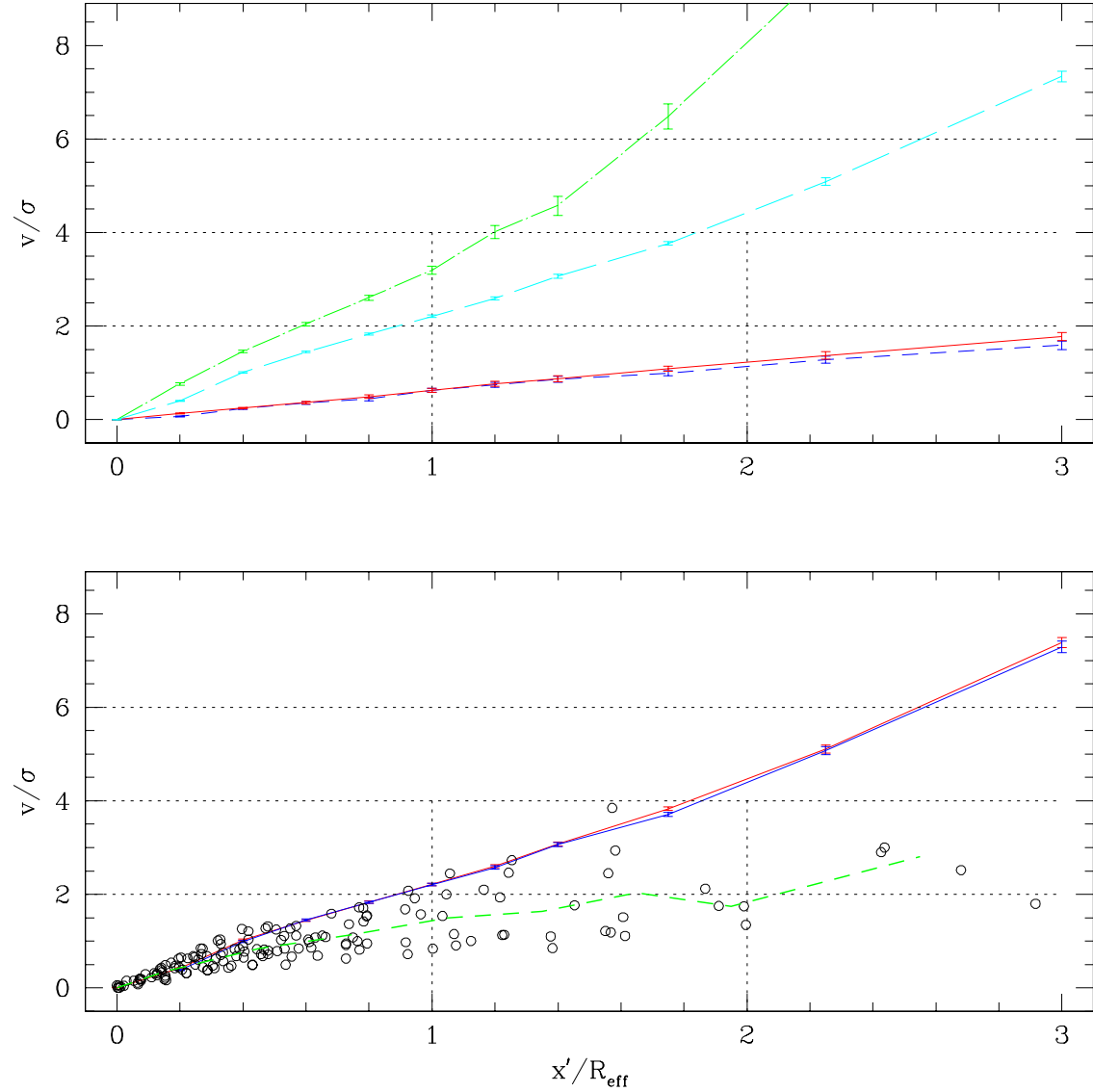


Fig. 9.— Bottom panel: temperature  $v/\sigma$  of the initial disk galaxy viewed edge-on (full line). The open dots are the individual  $v/\sigma$  of the R99 sample, while the dashed line is their mean  $\langle v/\sigma \rangle$  profile. Top panel: temperature  $v/\sigma$  of a cold disk (long dash-dotted line) and of our standard disk (long dashed line, see also bottom panel). The short-dashed line is the  $v/\sigma$  profile of the merger remnant initiated with this cold disk. For comparison, the full line is the remnant  $v/\sigma$  profile in case 1 (see table 1), which started from the (warmer) standard disk.